

Journal Pre-proof

Influence of QD photosensitizers in the photocatalytic production of hydrogen with biomimetic [FeFe]-hydrogenase. Comparative performance of CdSe and CdTe

Juan Corredor, Dulanjan Harankahage, Frederic Gloaguen, Maria J. Rivero, Mikhail Zamkov, Inmaculada Ortiz



PII: S0045-6535(21)00955-3

DOI: <https://doi.org/10.1016/j.chemosphere.2021.130485>

Reference: CHEM 130485

To appear in: *ECSN*

Received Date: 27 January 2021

Revised Date: 20 March 2021

Accepted Date: 2 April 2021

Please cite this article as: Corredor, J., Harankahage, D., Gloaguen, F., Rivero, M.J., Zamkov, M., Ortiz, I., Influence of QD photosensitizers in the photocatalytic production of hydrogen with biomimetic [FeFe]-hydrogenase. Comparative performance of CdSe and CdTe, *Chemosphere*, <https://doi.org/10.1016/j.chemosphere.2021.130485>.

This is a PDF file of an article that has undergone enhancements after acceptance, such as the addition of a cover page and metadata, and formatting for readability, but it is not yet the definitive version of record. This version will undergo additional copyediting, typesetting and review before it is published in its final form, but we are providing this version to give early visibility of the article. Please note that, during the production process, errors may be discovered which could affect the content, and all legal disclaimers that apply to the journal pertain.

© 2021 Published by Elsevier Ltd.

© 2021. This manuscript version is made available under the CC-BY-NC-ND 4.0 license <http://creativecommons.org/licenses/by-nc-nd/4.0/>

Author Contributions:

Conceptualization, J.C., M.J.R., I.O, F.G. and M.Z.

Methodology, J.C., M.J.R., I.O, D.H. and M.Z.

Validation, J.C., D.H. and M.Z.

Investigation, J.C. D.H. and M.Z.

Writing—original draft preparation, J.C.

Writing— review and editing J.C., M.J.R., I.O, F.G. and M.Z

Supervision, M.J.R., I.O. and M.Z.

Resources, M.J.R., I.O, F.G. and M.Z.

Project administration, M.J.R., I.O. and M.Z.

Funding acquisition, M.J.R., I.O. and M.Z.

J.C.: Juan Corredor

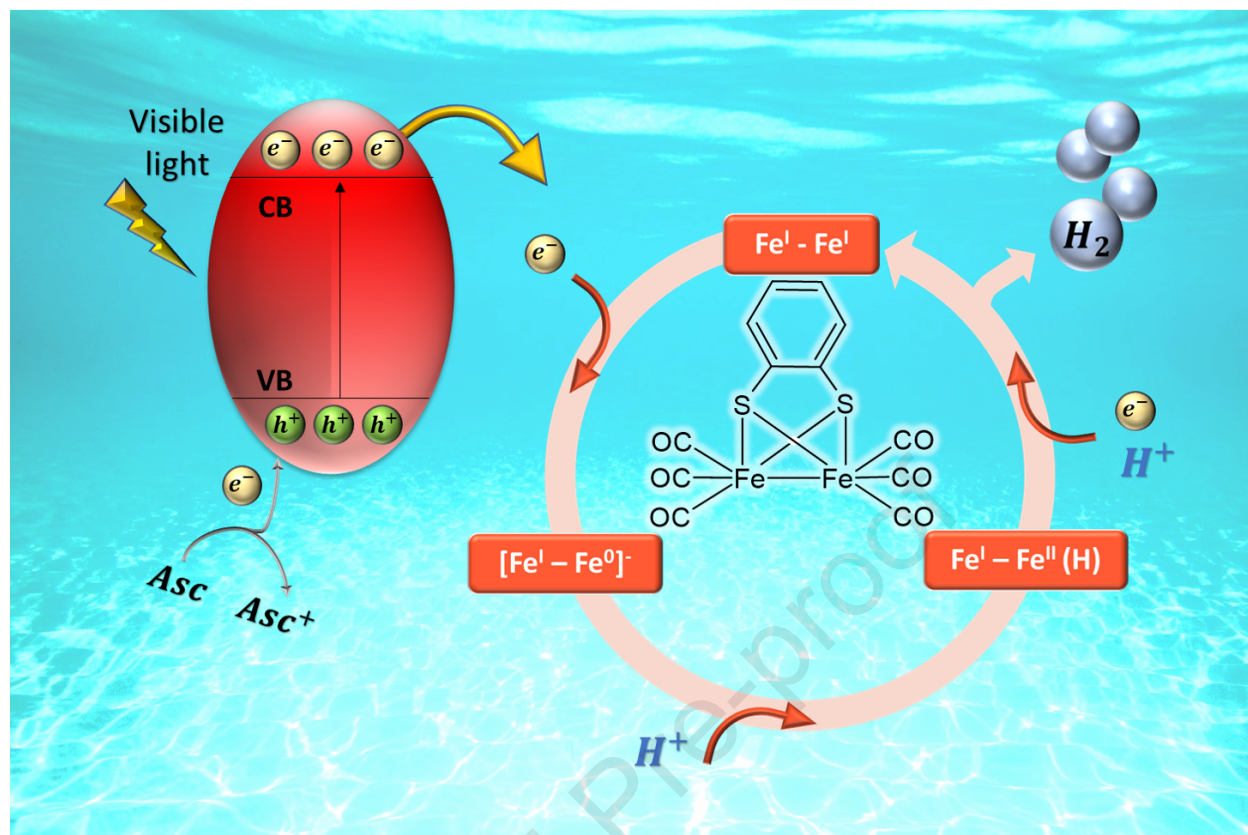
D.H.: Dulanjan Harankahage

F. G.: Frederic Gloaguen

M. J. R.: Maria J. Rivero

M. Z.: Mikhail Zamkov

I.O.: Inmaculada Ortiz



1 Influence of QD photosensitizers in the photocatalytic production
2 of hydrogen with biomimetic [FeFe]-hydrogenase. Comparative
3 performance of CdSe and CdTe

4 Juan Corredor ^a, Dulanjan Harankahage ^b, Frederic Gloaguen ^c, Maria J. Rivero ^a,
5 Mikhail Zamkov ^b, Inmaculada Ortiz ^{a*}

6 ^a Department of Chemical and Biomolecular Engineering, ETSIIT, University of
7 Cantabria, Avda. de los Castros s/n, 39005, Santander, Spain

8 ^b Department of Physics and Center for Photochemical Sciences, Bowling Green State
9 University, Bowling Green, Ohio 43043, USA

10 ^c UMR 6521, CNRS, Université de Bretagne Occidentale, CS 93837, 29238 Brest,
11 France

12 * Corresponding author. E-mail address: inmaculada.ortiz@unican.es (I. Ortiz)

13
14 Abstract

15 Photocatalytic systems comprising a hydrogenase-type catalyst and CdX (X = S, Se, Te)
16 chalcogenide quantum dot (QD) photosensitizers show extraordinary hydrogen
17 production rates under visible light excitation. What remains unknown is the
18 mechanism of energy conversion in these systems. Here, we have explored this question
19 by comparing the performance of two QD sensitizers, CdSe and CdTe, in photocatalytic
20 systems featuring aqueous suspensions of a [Fe₂(μ-1,2-benzenedithiolate) CO₆] catalyst
21 and an ascorbic acid sacrificial agent. Overall, the hydrogen production yield for CdSe-
22 sensitized reactions QDs was found to be 13 times greater than that of CdTe
23 counterparts. According to emission quenching experiments, an enhanced performance
24 of CdSe sensitizers reflected a greater rate of electron transfer from the ascorbic acid

25 (k_{As}). The observed difference in the QD-ascorbic acid charge transfer rates between
26 the two QD materials was consistent with respective driving forces for these systems.

27 **Keywords:** Photocatalytic hydrogen production, hydrogenase mimic, quantum dot,
28 CdSe, CdTe, electron transfer, hybrid systems.

29

30 1. Introduction

31 In the current global context, greenhouse gas emissions due to the combustion of fossil
32 fuels pose a threat to the global climate change (Hinojosa-Reyes et al., 2017; Fang et al.,
33 2018; Seadira et al., 2018). Therefore, research efforts have been directed towards
34 finding alternative and environmentally-friendly energy sources. In this context,
35 hydrogen appears as a clean energy vector whose combustion only produces water
36 (Chen et al., 2018; Munfarida et al., 2020; Oh et al., 2020). Nowadays, it is mainly
37 produced by steam reforming from fossil fuels (Chu et al., 2017; Nikolaidis and
38 Poullikkas, 2017; Corredor et al., 2020a). This process is energy intensive and plagued
39 by the emission of greenhouse gases (Holladay et al., 2009; Ribao et al., 2019). As a
40 result, the potential to produce hydrogen from alternative and greener technologies,
41 where electrolysis takes the leading role, is becoming increasingly important.
42 Complementarily, hydrogen can be released from residual gas or liquid effluents
43 through the use of cost-effective technologies, such as photocatalysis (Yue et al., 2017;
44 Nasir et al., 2019; Rivero et al., 2019). Photocatalysis is a way to harvest sunlight
45 energy and store it in the form of solar fuels, just as nature has done through natural
46 photosynthesis (Christoforidis and Fornasiero, 2017; El-Khouly et al., 2017; Zamkov,
47 2017; Giannoudis et al., 2020; Brillas et al., 2020).

48 As an alternative to noble metal catalysts, (Cho et al., 2021; Lai et al., 2021; Y. Yang et
49 al., 2021), recent studies have explored heterogeneous photocatalytic systems
50 comprising hydrogenases catalysts and semiconductor quantum dot (QD)
51 photosensitizers. The hydrogen production rates for these materials approaching 2 mmol
52 $\text{H}_2 \text{ g}_{\text{cat}}^{-1} \cdot \text{h}^{-1}$ were below those of homogeneous catalysts but showed an impressive long-
53 term stability (Putri et al., 2020; Elsayed et al., 2021; J. Yang et al., 2021).

54 Hydrogenase mimics is another promising noble metal-free catalyst that shows
55 compelling hydrogen production performance (Trincado et al., 2014; Fukuzumi et al.,
56 2018). Hydrogenases in nature are enzymes, which active sites are composed of Fe
57 and/or Ni, synthesized by certain bacteria and algae; these enzymes catalyze the
58 reversible redox reaction of H^+ to H_2 (Wang et al., 2012; Hemming et al., 2018; Li et al.,
59 2018). Among hydrogenases, [Fe-Fe]H₂-ases have shown a very high production
60 activity of hydrogen, about 6000-9000 H₂ molecules per second per active site (Stripp
61 and Happe, 2009; Li et al., 2018; Wittkamp et al., 2018; Wang et al., 2019). Therefore,
62 they have been studied in the last decades and have awakened interest in the synthesis
63 of biomimetic molecules (Capon et al., 2004; Liu and Darensbourg, 2007; Quentel et
64 al., 2012; Roy et al., 2013; Orain et al., 2014; Ahmed et al., 2018;).

65 [Fe-Fe]H₂-ases photocatalytic hydrogen production systems containing metal
66 complexes, such as $[\text{Ru}(\text{bpy})_3]^{2+}$ (bpy = 2,2'-bipyridine) or $[\text{Re}(4,4'$
67 dimethylbpy)(CO)₃]⁺ (Na et al., 2008; Streich et al., 2010; Wang et al., 2010; Pullen et
68 al., 2013; Yu et al., 2013) or organic dyes such as Eosin Y or Rose Bengal as
69 photosensitizers have been extensively studied (Li et al., 2012; Orain et al., 2014;
70 Supplis et al., 2018). Orain et al studied the photocatalytic hydrogen production in
71 aqueous solutions with [Fe-Fe]H₂-ase mimics, and organic dyes as photosensitizers
72 (Orain et al., 2014). Despite promising performance, their main drawback was the fast

73 excitation decay and the spectrally-narrow absorption band of dye sensitizers. In order
74 to overcome these issues, semiconductor QDs have been employed as photosensitizers
75 (Wang et al., 2011, 2013; Song et al., 2014; Liang et al., 2015; M. Wang et al., 2015;
76 Jian et al., 2016; Troppmann and König, 2016; Wen et al., 2016, 2017). Jian et al.
77 compared the performance of $[Ru(bpy)_3]^{2+}$ and CdSe QDs as a photosensitizer for the
78 same aqueous system achieving a hydrogen production rate of 301 and 20840 mmol
79 $H_2/g_{cat}^{-1}\cdot h^{-1}$, respectively, duplicating the stability of the system. Hydrogen production
80 was further enhanced by using a sacrificial agent that acted as an electron donor, such as
81 ascorbic acid (Fig. 1) (Goy et al., 2017).

82

83 Fig. 1. Hydrogen production by a [FeFe]H₂-ase mimic from ascorbic acid aqueous solution with
84 QDs as photosensitizer.

85

86 The selection of the QD material for sensitizing hydrogen production is still a challenge.

87 Cadmium chalcogenides, CdS, CdSe and CdTe, are good candidates due to their visible-

88 range absorbance and energetically favorable positions of band edges for driving the
89 hydrogen production processes (Hernandez-Ramirez et al., 2015). Since CdS absorbs
90 the smallest fraction of the solar energy, CdSe and CdTe QDs, exhibiting absorption in
91 the visible and near-IR, are usually preferred. For instance, CdSe has been used as
92 photosensitizer for hydrogen generation in combination with hydrogenases,
93 hydrogenase mimics, and even with bacteria that produce hydrogenases (Li et al., 2013;
94 Wang et al., 2013; Shen et al., 2013; Hamon et al., 2014; Liang et al., 2015; Jian et al.,
95 2016; Troppmann and König, 2016; Wen et al., 2016; Chica et al., 2017; Ding et al.,
96 2019; Sanchez et al., 2019a, 2019b; Li et al., 2020). CdTe has been also used for this
97 purpose (Brown et al., 2010; Wang et al., 2011; Greene et al., 2012; Jian et al., 2013;
98 Brown et al., 2014; Wroblewska-Wolna et al., 2020). Overall, the two QD sensitizers
99 appeared to perform differently in the presence of the same sacrificial agent and catalyst
100 components (Acharya et al., 2011; Brown et al., 2012), which makes this pair of QDs a
101 promising model system for interrogating energy conversion processes in sacrificial
102 hydrogen production reactions.

103 The present study offers a comprehensive analysis of the hydrogen production
104 performance for CdSe and CdTe QD photosensitizers under visible light irradiation.
105 The photocatalytic systems in present experiments featured a biomimetic hydrogenase
106 catalyst and ascorbic acid as a sacrificial agent. By drawing a comparison between the
107 two sensitizer QDs, we were able to infer that the primary rate-limiting step in these
108 systems is an electron transfer between the sacrificial agent and semiconductor QDs.
109 This conclusion was supported by cyclic voltammetry measurements showing a larger
110 difference between the oxidation potential of ascorbic acid and the valence band of
111 CdSe, as compared to CdTe.

112

113 2. Materials and methods

114 2.1. Materials

115 Oleic acid (OA) 90%, 1-octadene (ODE) 90%, trioctylphosphine oxide (TOPO),
116 cadmium oxide (CdO) 99.5%, tellurium powder 99.8% and tributylphosphine 97%
117 (TBP) were purchased from Sigma Aldrich. Chloroform and acetone were purchased
118 from ChemPure Chemicals. L-Ascorbic acid 98+% and methanol were provided by
119 Alfa Aesar. N-octadecylphosphonic acid (ODPA) was supplied by PCI.
120 Trioctylphosphine (TOP) was purchased from Strem Chemicals Inc. Selenium powder
121 99.99% was supplied by Beantown Chemicals. 3-mercaptopropionic acid (MPA) was
122 acquired from Acros Organics. Sodium dodecyl sulfate (SDS) 10% was provided by
123 LifeTechnologies.

124 2.2. Hydrogenase synthesis

125 $[\text{Fe}\chi(\mu\text{-}1,2\text{-benzenedithiolate})(\text{CO})_6]$, the $[\text{Fe-Fe}]_{\text{H}_2}$ -ase mimic, was synthesized as
126 previously described in the literature (Cabeza et al., 1998).

127 2.3. Synthesis of CdSe and CdTe quantum dots

128 OA-capped CdSe QDs were synthesized according to a procedure adapted from the
129 literature (Mongin et al., 2018). Briefly, OA-capped CdSe QDs were synthesized from
130 cadmium and selenium solutions. To prepare cadmium solution, 180 mg of CdO were
131 combined with 75 mg of ODPA, 9 g of TOPO and 6 mL of OA in a flask at 300 °C
132 under Ar atmosphere. When the solution turned clear, 5.4 mL of TOP were added.
133 Selenium solutions were prepared with 180 mg of Se powder and 3 mL of TOP at 140
134 °C under Ar atmosphere. After, the solution was cooled down to 80°C and it was
135 injected into the cadmium solution. The reaction time was 2 min. Every step was
136 performed under magnetic stirring.

137 To synthesize ODP A -capped CdTe QDs, the cadmium solution was prepared with 25.6
138 mg of CdO, 147.2 mg of ODP A and 8 mL of ODE at 300 °C under Ar atmosphere.
139 Tellurium solution was prepared from 51 mg of tellurium powder, 4 mL of ODE, and
140 0.46 mL of TBP at 80 °C under Ar atmosphere. Tellurium solution was injected into the
141 cadmium solution and the reaction was carried out for 4.75 min.

142 Both CdTe and CdSe suspensions were centrifuged for 4.5 min at 6500 rpm after adding
143 ethanol:acetone solution, with a volume ratio 2:1, to cause precipitation of the crystals.
144 The ratio between the crystals suspension and the ethanol-acetone mixture was 1:3 in
145 volume. The precipitated crystals were re-suspended in chloroform.

146 The ligand exchange process was carried out according to a procedure adapted from the
147 literature (Chang et al., 2016). Briefly, 0.5 mL of MPA were dissolved in 10 mL of a
148 1:1 methanol:chloroform solution at basic pH. 1.5 mL of crystals suspension were
149 added under constant stirring. QDs precipitated after centrifugation in acetone. They
150 were suspended in water and re-precipitated in acetone. Finally, the QDs were
151 suspended and stored in water.

152 2.4. Materials characterization

153 ^1H NMR spectra of $[\text{Fe}_2(\mu\text{-}1,2\text{-benzenedithiolate})(\text{CO})_6]$ in deuterated acetone were
154 recorded on a Bruker AC-300 FT-NMR spectrometer and were referenced against
155 SiMe_4 . The infrared spectra of $[\text{Fe}_2(\mu\text{-}1,2\text{-benzenedithiolate})(\text{CO})_6]$ in hexane were
156 recorded on a Nicolet Nexus FT-IR spectrometer.

157 The materials absorbance spectra were recorded in a UV-Vis spectrophotometer Cary
158 60 (Agilent). Photoluminescence spectra and excitation decay lifetime (τ_0) of CdSe and
159 CdTe QDs were obtained, exciting them with 405 nm PicoQuant PDL 800-D pulsed
160 laser and measuring their emission with an Andor Newton EM SR-303i-A spectrograph.

161 2.5. Hydrogen production

162 Hydrogen production experiments were carried out in an 8 mL reactor under magnetic
163 stirring. The reaction medium consisted of 4 mL of aqueous suspension with ascorbic
164 acid 200 mM (the amount of the sacrificial agent was used to assure excess of ascorbic
165 acid concentration during the experiments while avoiding the influence of its
166 concentration changes due to its consumption during the process), 0.1 mM of [Fe-
167 Fe]H₂-ase mimic, QDs in a concentration between 0.001 mM and 0.1 mM, and 10 mM
168 SDS sodium dodecyl sulfate (SDS) to solubilize the [Fe-Fe]H₂-ase mimic (Orain et al.,
169 2014; Supplis et al., 2018). The light source consisted of a 150 W halogen lamp,
170 provided with a filter which allowed only visible light to pass (400 nm < λ < 800 nm).
171 The irradiance on the reactor wall was 31 mW·cm⁻². It was measured with a Compact
172 Power and Energy Meter Console PM100D from Thorlabs. The concentration of
173 hydrogen was measured with a Shimadzu 8A gas chromatograph, equipped with a
174 thermal conductivity detector and a molecular sieve column 80/100 using argon as a
175 carrier gas. Hydrogen production experiments were performed at pH 4.5, which is close
176 to the ascorbic acid pK_a (4.2) (Tu et al., 2017); it has been reported that working close
177 to the sacrificial agent pK_a enhances hydrogen production (Corredor et al., 2019).

178

179 3. Results

180 The [Fe-Fe]H₂-ase mimic [Fe₂(μ-1,2-benzenedithiolate)(CO)₆] was characterized by
181 FTIR and ¹H-NMR spectroscopy. Three bands were displayed in the infrared spectra in
182 the ν_{CO} region: 2006, 2045 and 2079 cm⁻¹. ¹H-NMR (300 MHz, (CD₃)₂CO): δ 7.24 (m,
183 2H), 7.46 (m, 2H). These data are in good agreement with those reported by Cabeza et
184 al. (Cabeza et al., 1998). The [Fe-Fe]H₂-ase mimic absorbance spectra (Fig. SM-1)

185 showed an absorption peak at 330 nm and absorption at wavelengths lower than 300
186 nm. Therefore, the catalyst did not absorb radiation during hydrogen production
187 experiments, which were carried out using visible light excitation (400-800 nm).

188 The influence of the QD diameter on the effectiveness of hydrogen production with
189 hydrogenase enzymes has been investigated previously (Brown et al., 2014). In this
190 work, we only focus on single sizes of CdTe and CdSe QDs (2.95 and 2.68 nm,
191 respectively, see Fig. SM-2. Yu et al., 2003), which were chosen to enable similar
192 extinction values for the two sensitizers in the visible range. In this size range, the rate
193 of electron transfer to a catalysis was not expected to be influenced by the particle size
194 (Brown et al., 2014).

195 The UV-Vis absorbance and the emission spectra of the synthesized CdSe and CdTe
196 QDs before and after the ligand exchange process are shown in Fig. SM-3. Peng's
197 correlations were used to calculate the QD diameter from the spectral position of the
198 QD absorption edge (Yu et al., 2003). The QDs diameter was controlled via the reaction
199 time. A slight blue-shift was observed in the absorbance peak of both materials when
200 the hydrophobic ligands were exchanged with MPA.

201

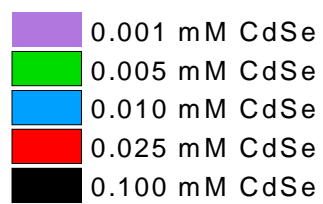
202 Fig. SM-4 shows the time-resolved luminescence decay curves of excited CdSe-OA,
203 CdSe-MPA, CdTe-ODPA and CdTe-MPA. The fluorescence intensity decay lifetime
204 (τ_0) was calculated by fitting the data to a three-phase exponential decay function (Gong
205 et al., 2013). The τ_0 values for CdSe-OA, CdSe-MPA, CdTe-ODPA and CdTe-MPA
206 were determined to be 38.4, 2.6, 14.7 and 9.6 ns, respectively. The value of τ_0 decreases
207 upon the ligand exchange with MPA for both materials. This decrease was previously
208 explained by the photoinduced hole transfer from a nanocrystal to MPA, which exhibits

209 a more negative energy relative to the semiconductor valence band (Ben-Shahar et al.,
210 2015; P. Wang et al., 2015).

211

212 3.2. Influence of Photosensitizer concentration on hydrogen production

213 Control tests were carried out in the absence of catalyst, in absence of photosensitizers
214 and with all components in the dark, successfully confirming the lack of hydrogen
215 production. In the next step, the influence of the CdSe QD concentration on hydrogen
216 production was investigated in the 0.001 mM to 0.1 mM range. The pH of the reaction
217 medium was the natural pH of the ascorbic acid (pKa 4.2) (Tu et al., 2017), as the
218 optimal pH for these systems has a value close to the pKa of the sacrificial agent. In
219 addition, Gloaguen and coworkers reported that a pH between 3 and 6 favored the
220 protonation of the electrochemically reduced [Fe-Fe]H₂-ase mimic leading to higher
221 hydrogen production (Quentel et al., 2012). The selected concentration of ascorbic acid
222 was 200 mM following previous reports (Jian et al., 2016). Fig. 2 shows that the highest
223 amount of hydrogen was produced using [CdSe] = 0.01 mM, giving a turnover number
224 (TON) of 18.3 mol of H₂ produced per mol of [Fe χ (μ -1,2-benzenedithiolate)(CO)₆]
225 during 3 h. The corresponding turnover number frequency (TOF), measured in mol of
226 produced H₂ per mol of catalyst per unit of time, was 6.5 h⁻¹. Under the conditions of
227 this study, the generated hydrogen increased with the QD concentration up to a
228 maximum value obtained at a concentration of CdSe 0.01M, and after that it decreased
229 as the concentration of the QD increased.

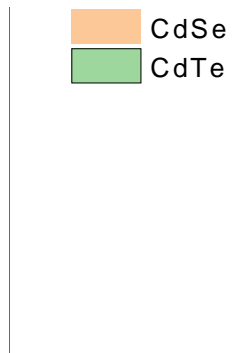


Journal Pre-proof

245 inefficient activation of the photosensitizer particles. This is clarified by equation S6,
246 which shows that the irradiation of the light source strongly influences the optimal
247 concentration of the photosensitizer because the number of excited particles depends on
248 the number of accessible photons.

249 3.3. Comparative performance of the photosensitizers CdSe and CdTe

250 In order to compare the performance of photosensitizers MPA-CdSe and MPA-CdTe,
251 experiments were carried out with a concentration 0.01 mM of each photosensitizer.
252 Fig. 3 shows the data of hydrogen production expressed as TON with CdSe and CdTe
253 during 3 h. Under similar experimental conditions, a TOF of 6.5 h^{-1} was observed with
254 CdSe, which is 13-fold higher than with CdTe (TOF = 0.5 h^{-1}). Table S1 collects the
255 values of the total hydrogen production and the production rate. The reported TOF
256 values for aqueous systems with ascorbic acid as sacrificial agent, MPA-capped CdSe
257 or CdTe QDs as photosensitizers and natural or biomimetic [Fe-Fe] H_2 -ase as catalyst,
258 are included in Table SM-2. Although TOF values reached in this work are smaller
259 than other values reported in literature, it is worth noting that reported data have been
260 obtained by working with different concentrations of catalyst and different light
261 irradiation, making it difficult to extract precise conclusions. However, it is interesting
262 to note that the system proposed in this work exhibited higher stability than other
263 systems exhibiting greater TOF.



Journal Pre-proof

268

269 Fig. 4. Emission spectra at different concentrations of (a) catalyst in CdSe-MPA medium; (b)
270 catalyst in CdTe-MPA medium; (c) ascorbic acid in CdSe-MPA medium; (d) ascorbic acid in
271 CdTe-MPA medium.

272

273 Emission quenching spectra with progressive addition of catalyst and ascorbic acid to
274 CdSe-MPA and CdTe-MPA media are shown in Fig. 4. According to Fig. 4a and 4b,
275 addition of a catalyst causes a decrease in the fluorescence intensity, which is consistent
276 with the transfer of photoexcited electrons from CdSe/CdTe to the catalyst. The
277 comparison of the UV-Vis spectrum of $[\text{Fe}_2(\mu\text{-}1,2\text{-benzenedithiolate})(\text{CO})_6]$ (Fig. SM-
278 1), which shows an absorption peak around 340 nm, with the emission spectra of CdSe
279 and CdTe showing maxima around 545 and 540 nm, respectively (Fig. SM-3), leads to
280 the conclusion that the catalyst does not absorb the fluorescence emitted by the
281 photosensitizer. Thus, the loss of fluorescence intensity is due to the transfer of
282 electrons from the conduction band of the photosensitizer to the catalyst. Consequently,
283 the quenching constant (k_q), calculated using the Stern-Volmer equation (Fig. SM-9)

284 (Stern and Volmer, 1919), is equal to the rate constant of electron transfer from the
285 photosensitizer to the catalyst (k_{ET}), $k_q = k_{ET}$, with values of $1.55 \cdot 10^{12}$ and $4.02 \cdot 10^{11} \text{ M}^{-1}$
286 $\cdot \text{s}^{-1}$ for CdSe and CdTe, respectively. Similarly, quenching of fluorescence was also
287 observed with increasing concentration of the ascorbic acid (scavenger) in medium (see
288 Fig. 4c and 4d). Since there is no overlap between the ascorbic acid absorption (Fig.
289 SM-8) and the photosensitizer emission (Fig. SM-3), it was concluded that the
290 quenching effect is due to the transfer of electrons from ascorbic acid to the
291 photosensitizer valence band. In this case, the rate constant of electron transfer from
292 ascorbic acid to the photosensitizer (k_{asc}), was found to be $5.42 \cdot 10^9$ and $4.31 \cdot 10^8 \text{ M}^{-1} \cdot \text{s}^{-1}$
293 for CdSe and CdTe, respectively.

294 A difference of 2-3 orders of magnitude was observed between k_{ET} and k_{asc} in both
295 materials. This difference agrees with previous reports (Jian et al., 2016; Wen et al.,
296 2016). Fig. 5 depicts the proposed mechanism where the acceptance of the electrons
297
298 limiting step as k_{asc} is two orders of magnitude smaller than k_{ET} . Furthermore, CdSe
299 sensitizer showed a greater k_{asc} which was nearly 13 times higher than for CdTe. This
300 fact is consistent with the 13 times greater hydrogen production rate obtained with CdSe
301 than with CdTe. Therefore, it was concluded that the electron transfer from the ascorbic
302 acid to the QD was the primary rate-limiting step in hydrogen production reactions.

303

304 Fig. 5. Mechanism of photocatalytic hydrogen production.

305

306 Fig. 6 represents the energy diagram of both systems at pH 4.5. The reduction potential
307 of the [Fe-Fe]H₂-ase mimic was determined by cyclic voltammetry as $E_{1/2} \sim -0.68$ V at
308 pH 4.5 (Quentel et al., 2012) and for ascorbic acid the corresponding value was -0.41 V
309 (Tu et al., 2017). Although it is energetically favorable for the ascorbic acid to produce
310 hydrogen directly, it was confirmed experimentally that this redox reaction did not
311 occur. For both semiconductors, Fig. 6 illustrates the conduction and valence band edge
312 energies for CdSe and CdTe QDs adjusted for present particle diameters considering the
313 variability range found in literature. (Jasieniak et al., 2011). Notably, the energy
314 difference between the oxidation potential of ascorbic acid and the valence band of the
315 QD is greater for CdSe than for CdTe, which is consistent with the higher value of k_{Ac}
316 of CdSe with respect to CdTe. This causes a comparatively greater driving force for the
317 photoinduced electron transfer from sacrificial agent to the CdSe.

318

319 Fig. 6. Energy levels at pH 4.5 of CdSe, CdTe, [FeFe]H₂-ase mimic and ascorbic acid.

320

321 Overall, the above experiments demonstrate that the rate-limiting step for the hydrogen
322 production in the QD-([FeFe]H₂-ase mimic)-(ascorbic acid) system is the electron
323 transfer from the ascorbic acid (sacrificial agent) to the valence band of the
324 photosensitizer characterized by the kinetic constant k_{Asc} .

325 In an effort to assess the stability of the investigated catalytic system, several selected
326 experiments were carried out for the duration of 24 h. According to Fig. 7a, CdSe
327 reached a TON value of 100 while CdTe achieved a TON value of 3.5 after 24 h. The
328 initial TOF with CdSe was 6.5 h^{-1} decreasing to 1.8 h^{-1} after 18 h while the initial TOF
329 with CdTe was 0.5 h^{-1} decreasing to 0.1 h^{-1} after 18 h. Therefore, hydrogen production
330 rate decreased about 75% for both materials in this period of time. Fig. 7b shows
331 hydrogen production with CdSe operating in different cycles. Cycle 1 shows hydrogen
332 production with a fresh catalyst. Hydrogen production rate decreased to 1.8 h^{-1} after 18 h
333 of reaction. Before starting cycle 2, a purge with argon was carried out in the
334 photoreactor to eliminate any possible inhibitory effect of the product, as has been
335 previously reported (Corredor et al., 2020b). After this purge, the TOF was 1.7 h^{-1} ,
336 similar to the value at the end of cycle 1. Therefore, the decrease in hydrogen
337 production was not attributed to the hydrogen inhibitory effect. Next, catalyst
338 deactivation was examined by addition of $7.5 \cdot 10^{-3} \text{ mM}$ of fresh catalyst at the beginning
339 of cycle 3; hydrogen production recovered similar values to the initial experimental
340 conditions. Therefore, the decline and stop of hydrogen production is attributed to the
341 loss of catalyst activity.

Journal Pre-proof

342

343 Fig. 7. Hydrogen production with (a) CdSe and CdTe for longer operation times, and (b) catalyst
344 reuse with CdSe.

345

346 4. Conclusions

347 In this work, we compare the photocatalytic performance of two QD photosensitizers,

348 CdSe and CdTe, in hydrogen production systems composed of a hydrogenase mimic

349 catalyst and ascorbic acid as sacrificial agent. CdSe QDs showed an overall better

350 performance. For these materials, the highest hydrogen production rate was observed

351 using 0.01 mM nanoparticle concentration, 200 mM of ascorbic acid, and 0.1 mM of
352 [Fe-Fe]H₂-ase mimic (excitation intensity = 31 mW·cm⁻² of, 400 nm < λ < 800 nm).
353 Quenching experiments revealed that the rate of electron transfer from photosensitizer
354 to the catalyst, k_{ET}, is of 2-3 orders of magnitude higher than that of sacrificial agent→
355 photosensitizer transfer process, k_{asc}. In particular, we found that k_{asc} for CdSe was 13
356 times greater than that of CdTe. The ratio of hydrogen production rates for the two
357 materials, CdSe and CdTe, exhibited roughly the same value (13:1), suggesting that the
358 acceptance of the electrons from the ascorbic acid by the photogenerated holes in the
359 QD's valence band was the rate limiting step. A relatively greater value of k_{asc} for CdSe
360 was attributed to the larger difference between the oxidation potential of ascorbic acid
361 and the valence band energy of CdSe in comparison with CdTe. This conclusion
362 suggests that photosensitizers that enable faster sacrificial regenerations may hold the
363 key to improving the hydrogen production rate. A nother important area to be addressed
364 by the future research is the long-term stability of hydrogenase mimic catalysts, which
365 lost 25% of catalytic activity after 18 h in present measurements.

366

367 5. Acknowledgements

368 Financial support from projects RTI2018-099407-B-I00, RTI2018-093310-B-I00,
369 RTC2019-006820-5 (MCIU/AEI/FEDER, UE) and 'HYLANTIC'-EAPA_204/2016
370 (Interreg Atlantic/FEDER UE) is gratefully acknowledged. Juan Corredor is grateful to
371 FPI contract grant (BES-2016-079201). MZ and DH were supported by the Award DE-
372 SC0016872 (MZ) funded by the U.S. Department of Energy, Office of Science.

373

374 6. References

- 375 Acharya, K.P., Khnayzer, R.S., O'Connor, T., Diederich, G., Kirsanova, M., Klinkova,
376 A., Roth, D., Kinder, E., Imboden, M., Zamkov, M., 2011. The role of hole
377 localization in sacrificial hydrogen production by semiconductor-metal
378 heterostructured nanocrystals. *Nano Lett.* 11, 2919–2926.
379 <https://doi.org/10.1021/nl201388c>
- 380 Ahmed, M.E., Dey, S., Darensbourg, M.Y., Dey, A., 2018. Oxygen-Tolerant H₂
381 Production by [FeFe]-H₂ase Active Site Mimics Aided by Second Sphere Proton
382 Shuttle. *J. Am. Chem. Soc.* 140, 12457–12468.
383 <https://doi.org/10.1021/jacs.8b05983>
- 384 Baker, D.R., Kamat, P. V., 2010. Tuning the emission of CdSe Quantum Dots by
385 Controlled Deep-Trap Enhancement. *Langmuir* 26, 11272–11276.
- 386 Ben-Shahar, Y., Scotognella, F., Waiskopf, N., Kriegel, I., Dal Conte, S., Cerullo, G.,
387 Banin, U., 2015. Effect of surface coating on the photocatalytic function of hybrid
388 CdS-Au nanorods. *Small* 11, 462–471. <https://doi.org/10.1002/smll.201402262>
- 389 Brillas, E., Serrà, A., Garcia-Segura, S., 2021. Biomimicry designs for
390 photoelectrochemical systems: Strategies to improve light delivery efficiency.
391 *Curr. Opin. Electrochem.* 26, 100660. <https://doi.org/10.1016/j.coelec.2020.100660>
- 392 Brown, K.A., Dayal, S., Ai, X., Rumbles, G., King, P.W., 2010. Controlled assembly of
393 hydrogenase-CdTe nanocrystal hybrids for solar hydrogen production. *J. Am.*
394 *Chem. Soc.* 132, 9672–9680. <https://doi.org/10.1021/ja101031r>
- 395 Brown, K.A., Song, Q., Mulder, D.W., King, P.W., 2014. Diameter dependent electron
396 transfer kinetics in semiconductor-enzyme complexes. *ACS Nano* 8, 10790–10798.
397 <https://doi.org/10.1021/nn504561v>

- 398 Brown, K.A., Wilker, M.B., Boehm, M., Dukovic, G., King, P.W., 2012.
399 Characterization of photochemical processes for H₂ production by CdS nanorod-
400 [FeFe] hydrogenase complexes. *J. Am. Chem. Soc.* 134, 5627–5636.
401 <https://doi.org/10.1021/ja2116348>
- 402 Cabeza, J.A., Martínez-García, M.A., Riera, V., Ardura, D., García-Granda, S., 1998.
403 Binuclear iron(I), ruthenium(I), and osmium(I) hexacarbonyl complexes containing
404 a bridging benzene-1,2-dithiolate ligand. Synthesis, X-ray structures, protonation
405 reactions, and EHMO calculations. *Organometallics* 17, 1471–1477.
406 <https://doi.org/10.1021/om970922j>
- 407 Capon, J.F., Gloaguen, F., Schollhammer, P., Talarmin, J., 2004. Electrochemical
408 proton reduction by thiolate-bridged hexacarbonyldiiron clusters. *J. Electroanal.*
409 *Chem.* 566, 241–247. <https://doi.org/10.1016/j.jelechem.2003.11.032>
- 410 Chang, C.M., Orchard, K.L., Martindale, B.C.M., Reisner, E., 2016. Ligand removal
411 from CdS quantum dots for enhanced photocatalytic H₂ generation in pH neutral
412 water. *J. Mater. Chem. A* 4, 2856–2862. <https://doi.org/10.1039/c5ta04136h>
- 413 Chen, Y., Xiao, K., Shen, N., Zeng, R.J., Zhou, Y., 2018. Hydrogen production from a
414 thermophilic alkaline waste activated sludge fermenter: Effects of solid retention
415 time (SRT). *Chemosphere* 206, 101–106.
416 <https://doi.org/10.1016/j.chemosphere.2018.04.170>
- 417 Chica, B., Wu, C.H., Liu, Y., Adams, M.W.W., Lian, T., Dyer, R.B., 2017. Balancing
418 electron transfer rate and driving force for efficient photocatalytic hydrogen
419 production in CdSe/CdS nanorod-[NiFe] hydrogenase assemblies. *Energy Environ.*
420 *Sci.* 10, 2245–2255. <https://doi.org/10.1039/c7ee01738c>
- 421 Cho, H., Joo, H., Kim, H., Kim, J.E., Kang, K.S., Yoon, J., 2021. Improved

- 422 photoelectrochemical properties of TiO₂ nanotubes doped with Er and effects on
423 hydrogen production from water splitting. *Chemosphere* 267, 129289.
424 <https://doi.org/10.1016/j.chemosphere.2020.129289>
- 425 Christoforidis, K.C., Fornasiero, P., 2017. Photocatalytic Hydrogen production: A rift
426 into the future energy supply. *ChemCatChem* 9, 1523–1544.
427 <https://doi.org/10.1002/cctc.201601659>
- 428 Chu, K.H., Ye, L., Wang, W., Wu, D., Chan, D.K.L., Zeng, C., Yip, H.Y., Yu, J.C.,
429 Wong, P.K., 2017. Enhanced photocatalytic hydrogen production from aqueous
430 sulfide/sulfite solution by ZnO₆S₀₄ with simultaneous dye degradation under
431 visible-light irradiation. *Chemosphere* 183, 219–228.
432 <https://doi.org/10.1016/j.chemosphere.2017.05.112>
- 433 Corredor, J., Perez-Peña, E., Rivero, M.J., Ortiz, I., 2020a. Performance of rGO/TiO₂
434 photocatalytic membranes for hydrogen production. *Membranes* 10, 1–13.
435 <https://doi.org/10.3390/membranes10090218>
- 436 Corredor, J., Rivero, M.J., Ortiz, I., 2020b. New insights in the performance and reuse
437 of rGO/TiO₂ composites for the photocatalytic hydrogen production. *Int. J.*
438 *Hydrogen Energy* (In press). <https://doi.org/10.1016/j.ijhydene.2020.01.181>
- 439 Corredor, J., Rivero, M.J., Rangel, C.M., Gloaguen, F., Ortiz, I., 2019. Comprehensive
440 review and future perspectives on the photocatalytic hydrogen production. *J.*
441 *Chem. Technol. Biotechnol.* 94, 3049–3063. <https://doi.org/10.1002/jctb.6123>
- 442 Ding, Y., Bertram, J.R., Eckert, C., Bommarreddy, R.R., Patel, R., Conradie, A., Bryan,
443 S., Nagpal, P., 2019. Nanorg Microbial Factories: Light-Driven Renewable
444 Biochemical Synthesis Using Quantum Dot-Bacteria Nanobiohybrids. *J. Am.*
445 *Chem. Soc.* 141, 10272–10282. <https://doi.org/10.1021/jacs.9b02549>

- 446 El-Khouly, M.E., El-Mohsnawy, E., Fukuzumi, S., 2017. Solar energy conversion:
447 From natural to artificial photosynthesis. *J. Photochem. Photobiol. C Photochem.*
448 *Rev.* 31, 36–83. <https://doi.org/10.1016/j.jphotochemrev.2017.02.001>
- 449 Elsayed, M.H., Jayakumar, J., Abdellah, M., Mansoure, T.H., Zheng, K., Elewa, A.M.,
450 Chang, C.L., Ting, L.Y., Lin, W.C., Yu, H., Wang, W.H., Chung, C.-C., Chou, H.-
451 H., 2021. Visible-light-driven hydrogen evolution using nitrogen-doped carbon
452 quantum dot-implanted polymer dots as metal-free photocatalysts. *Appl. Catal. B*
453 *Environ.* 283, 119659. <https://doi.org/10.1016/j.apcatb.2020.119659>
- 454 Fang, X., Cui, L., Pu, T., Song, J., Zhang, X., 2018. Core-shell CdS@MnS nanorods as
455 highly efficient photocatalysts for visible light driven hydrogen evolution. *Appl.*
456 *Surf. Sci.* 457, 863–869. <https://doi.org/10.1016/j.apsusc.2018.07.012>
- 457 Fukuzumi, S., Lee, Y.M., Nam, W., 2018. Thermal and photocatalytic production of
458 hydrogen with earth-abundant metal complexes. *Coord. Chem. Rev.* 355, 54–73.
459 <https://doi.org/10.1016/j.ccr.2017.07.014>
- 460 Giannoudis, E., Benazzi, E., Karlsson, J., Copley, G., Panagiotakis, S., Landrou, G.,
461 Angaridis, P., Nikolaou, V., Matthaiaki, C., Charalambidis, G., Gibson, E.A.,
462 Coutsolelos, A.G., 2020. Photosensitizers for H₂ Evolution Based on Charged or
463 Neutral Zn and Sn Porphyrins. *Inorg. Chem.* 59, 1611–1621.
464 <https://doi.org/10.1021/acs.inorgchem.9b01838>
- 465 Gong, K., Zeng, Y., Kelley, D.F., 2013. Extinction coefficients, oscillator strengths, and
466 radiative lifetimes of CdSe, CdTe, and CdTe/CdSe nanocrystals. *J. Phys. Chem. C*
467 117, 20268–20279. <https://doi.org/10.1021/jp4065449>
- 468 Goy, R., Bertini, L., Rudolph, T., Lin, S., Schulz, M., Zampella, G., Dietzek, B.,
469 Schacher, F.H., De Gioia, L., Sakai, K., Weigand, W., 2017. Photocatalytic

- 470 Hydrogen Evolution Driven by [FeFe] Hydrogenase Models Tethered to Fluorene
471 and Silafluorene Sensitizers. *Chem. Eur. J.* 23, 334–345.
472 <https://doi.org/10.1002/chem.201603140>
- 473 Greene, B.L., Joseph, C.A., Maroney, M.J., Dyer, R.B., 2012. Direct evidence of active-
474 site reduction and photodriven catalysis in sensitized hydrogenase assemblies. *J.*
475 *Am. Chem. Soc.* 134, 11108–11111. <https://doi.org/10.1021/ja3042367>
- 476 Hamon, C., Ciaccafava, A., Infossi, P., Puppo, R., Even-Hernandez, P., Lojou, E.,
477 Marchi, V., 2014. Synthesis and enzymatic photo-activity of an O₂tolerant
478 hydrogenase-CdSe@CdS quantum rod bioconjugate. *Chem. Commun.* 50, 4989–
479 4992. <https://doi.org/10.1039/c3cc49368g>
- 480 Hemming, E.B., Chan, B., Turner, P., Corcilius, L., Price, J.R., Gardiner, M.G.,
481 Masters, A.F., Maschmeyer, T., 2018. [Fe(C₅Ar₅)(CO)₂Br] complexes as
482 hydrogenase mimics for the catalytic hydrogen evolution reaction. *Appl. Catal. B*
483 *Environ.* 223, 234–241. <https://doi.org/10.1016/j.apcatb.2017.04.053>
- 484 Hernandez-Ramirez, A., Medina-Ramirez, I., 2015. Semiconducting materials, in:
485 Hernandez-Ramirez, A., Medina-Ramirez, I. (Eds.), *Photocatalytic*
486 *Semiconductors*. Springer, 1–40. [https://doi.org/https://doi.org/10.1007/978-3-319-](https://doi.org/https://doi.org/10.1007/978-3-319-10999-2_1)
487 [10999-2_1](https://doi.org/10.1007/978-3-319-10999-2_1)
- 488 Hinojosa-Reyes, M., Camposeco-Solís, R., Zanella, R., Rodríguez González, V., 2017.
489 Hydrogen production by tailoring the brookite and Cu₂O ratio of sol-gel Cu-TiO₂
490 photocatalysts. *Chemosphere* 184, 992–1002.
491 <https://doi.org/10.1016/j.chemosphere.2017.06.066>
- 492 Holladay, J.D., Hu, J., King, D.L., Wang, Y., 2009. An overview of hydrogen
493 production technologies. *Catal. Today* 139, 244–260.

- 494 <https://doi.org/10.1016/j.cattod.2008.08.039>
- 495 Jasieniak, J., Califano, M., Watkins, S.E., 2011. Size-dependent valence and conduction
496 band-edge energies of semiconductor nanocrystals. *ACS Nano* 5, 5888–5902.
497 <https://doi.org/10.1021/nn201681s>
- 498 Jian, J.X., Liu, Q., Li, Z.J., Wang, F., Li, X.B., Li, C.B., Liu, B., Meng, Q.Y., Chen, B.,
499 Feng, K., Tung, C.H., Wu, L.Z., 2013. Chitosan confinement enhances hydrogen
500 photogeneration from a mimic of the diiron subsite of [FeFe]-hydrogenase. *Nat.*
501 *Commun.* 4, 2695. <https://doi.org/10.1038/ncomms3695>
- 502 Jian, J.X., Ye, C., Wang, X.-Z., Wen, M., Li, Z.-J., Li, X.-B., Chen, B., Tung, C.-H.,
503 Wu, L.-Z., 2016. Comparison of H₂ photogeneration by [FeFe]-hydrogenase
504 mimics with CdSe QDs and Ru(bpy)₃Cl₂ in aqueous solution. *Energy Environ. Sci.*
505 9, 2083–2089. <https://doi.org/10.1039/C6EE00629A>
- 506 Lai, G.J., Lyu, L.M., Huang, Y.S., Lee, G.C., Lu, M.P., Perng, T.P., Lu, M.Y., Chen,
507 L.J., 2021. Few-layer WS₂-MoS₂ in-plane heterostructures for efficient
508 photocatalytic hydrogen evolution. *Nano Energy* 81, 105608.
509 <https://doi.org/10.1016/j.nanoen.2020.105608>
- 510 Li, C.B., Li, Z.J., Yu, S., Wang, G.X., Wang, F., Meng, Q.Y., Chen, B., Feng, K., Tung,
511 C.H., Wu, L.Z., 2013. Interface-directed assembly of a simple precursor of [FeFe]-
512 H₂ase mimics on CdSe QDs for photosynthetic hydrogen evolution in water.
513 *Energy Environ. Sci.* 6, 2597–2602. <https://doi.org/10.1039/c3ee40992a>
- 514 Li, R.X., Ren, X.T., Tang, M.Y., Chen, M.X., Huang, G.B., Fang, C.H., Liu, T., Feng,
515 Z.H., Yin, Y.B., Guo, Y.M., Mei, S.K., Yan, J., 2018. Fabrication of covalently
516 linked graphene-mediated [FeFe]-hydrogenases biomimetic photocatalytic
517 hydrogen evolution system in aqueous solution. *Appl. Catal. B Environ.* 224, 772–

- 518 782. <https://doi.org/10.1016/j.apcatb.2017.09.062>
- 519 Li, X., Wang, M., Chen, L., Wang, X., Dong, J., Sun, L., 2012. Photocatalytic water
520 reduction and study of the formation of $\text{Fe}^{\text{I}}\text{Fe}^{\text{0}}$ species in diiron catalyst systems.
521 *ChemSusChem* 5, 913–919. <https://doi.org/10.1002/cssc.201100490>
- 522 Li, X.B., Jian, J.X., Wang, X.Z., Wang, Y., Xia, S.G., Tung, C.H., Wu, L.Z., 2020. Per-
523 6-Thiol-Cyclodextrin Engineered [FeFe]-Hydrogenase Mimic/CdSe Quantum Dot
524 Assembly for Photocatalytic Hydrogen Production. *Sol. RRL* (In press).
525 <https://doi.org/10.1002/solr.202000474>
- 526 Liang, W.J., Wang, F., Wen, M., Jian, J.X., Wang, X.Z., Chen, B., Tung, C.H., Wu,
527 L.Z., 2015. Branched polyethylenimine improves hydrogen photoproduction from
528 a CdSe quantum dot/[FeFe]-hydrogenase mimic system in neutral aqueous
529 solutions. *Chem. Eur. J.* 21, 3187–3192. <https://doi.org/10.1002/chem.201406361>
- 530 Liu, T., Darensbourg, M.Y., 2007. A mixed-valent, Fe(II)Fe(I), diiron complex
531 reproduces the unique rotated state of the [FeFe]hydrogenase active site. *J. Am.*
532 *Chem. Soc.* 129, 7008–7009. <https://doi.org/10.1021/ja071851a>
- 533 Lyon, E.J., Georgakaki, I.P., Reibenspies, J.H., Darensbourg, M.Y., 2001. Coordination
534 sphere flexibility of active-site models for Fe-only hydrogenase: Studies in intra-
535 and intermolecular diatomic ligand exchange. *J. Am. Chem. Soc.* 123, 3268–3278.
536 <https://doi.org/10.1021/ja003147z>
- 537 Mongin, C., Moroz, P., Zamkov, M., Castellano, F.N., 2018. Thermally activated
538 delayed photoluminescence from pyrenyl-functionalized CdSe quantum dots. *Nat.*
539 *Chem.* 10, 225–230. <https://doi.org/10.1038/nchem.2906>
- 540 Munfarida, S., Widayat, Satriadi, H., Cahyono, B., Hadiyanto, Philia, J., Prameswari, J.,

- 541 2020. Geothermal industry waste-derived catalyst for enhanced biohydrogen
542 production. *Chemosphere* 258, 127274.
543 <https://doi.org/10.1016/j.chemosphere.2020.127274>
- 544 Na, Y., Wang, M., Pan, J., Zhang, P., Åkermark, B., Sun, L., 2008. Visible light-driven
545 electron transfer and hydrogen generation catalyzed by bioinspired [2Fe2S]
546 complexes. *Inorg. Chem.* 47, 2805–2810. <https://doi.org/10.1021/ic702010w>
- 547 Nasir, M.S., Yang, G., Ayub, I., Wang, S., Wang, L., Wang, X., Yan, W., Peng, S.,
548 Ramakarishna, S., 2019. Recent development in graphitic carbon nitride based
549 photocatalysis for hydrogen generation. *Appl. Catal. B Environ.* 257, 117855.
550 <https://doi.org/10.1016/j.apcatb.2019.117855>
- 551 Nikolaidis, P., Poullikkas, A., 2017. A comparative overview of hydrogen production
552 processes. *Renew. Sustain. Energy Rev.* 67, 597–611.
553 <https://doi.org/10.1016/j.rser.2016.09.044>
- 554 Oh, W.C., Nguyen, D.C.T., Areerob, Y., 2020. Novel cadmium oxide-graphene
555 nanocomposite grown on mesoporous silica for simultaneous photocatalytic H₂-
556 evolution. *Chemosphere* 239, 124825.
557 <https://doi.org/10.1016/j.chemosphere.2019.124825>
- 558 Orain, C., Quentel, F., Gloaguen, F., 2014. Photocatalytic Hydrogen Production Using
559 Models of the Iron-Iron Hydrogenase Active Site Dispersed in Micellar Solution.
560 *ChemSusChem* 7, 638–643. <https://doi.org/10.1002/cssc.201300631>
- 561 Pullen, S., Fei, H., Orthaber, A., Cohen, S.M., Ott, S., 2013. Enhanced photochemical
562 hydrogen production by a molecular diiron catalyst incorporated into a metal-
563 organic framework. *J. Am. Chem. Soc.* 135, 16997–17003.
564 <https://doi.org/10.1021/ja407176p>

- 565 Putri, L.K., Ng, B.J., Ong, W.J., Lee, H.W., Chang, W.S., Mohamed, A.R., Chai, S.P.,
566 2020. Energy level tuning of CdSe colloidal quantum dots in ternary 0D-2D-2D
567 CdSe QD/B-rGO/O-gC₃N₄ as photocatalysts for enhanced hydrogen generation.
568 Appl. Catal. B Environ. 265, 118592. <https://doi.org/10.1016/j.apcatb.2020.118592>
- 569 Quentel, F., Passard, G., Gloaguen, F., 2012. Electrochemical hydrogen production in
570 aqueous micellar solution by a diiron benzenedithiolate complex relevant to [FeFe]
571 hydrogenases. Energy Environ. Sci. 5, 7757–7761.
572 <https://doi.org/10.1039/c2ee21531d>
- 573 Ribao, P., Alexandra Esteves, M., Fernandes, V.R., Rivero, M.J., Rangel, C.M., Ortiz,
574 I., 2019. Challenges arising from the use of TiO₂/rGO/Pt photocatalysts to produce
575 hydrogen from crude glycerol compared to synthetic glycerol. Int. J. Hydrogen
576 Energy 44, 28494–28506.
577 <https://doi.org/https://doi.org/10.1016/j.ijhydene.2018.09.148>
- 578 Rivero, M.J., Iglesias, O., Ribao, P., Ortiz, I., 2019. Kinetic performance of
579 TiO₂/Pt/reduced graphene oxide composites in the photocatalytic hydrogen
580 production. Int. J. Hydrogen Energy 44, 101–109.
581 <https://doi.org/10.1016/j.ijhydene.2018.02.115>
- 582 Roy, S., Groy, T.L., Jones, A.K., 2013. Biomimetic model for [FeFe]-hydrogenase:
583 asymmetrically disubstituted diiron complex with a redox-active 2,2'-bipyridyl
584 ligand. Dalt. Trans. 42, 3843–3853. <https://doi.org/10.1039/c2dt32457a>
- 585 Sanchez, M.L.K., Sommer, C., Reijerse, E., Birrell, J.A., Lubitz, W., Dyer, R.B., 2019a.
586 Investigating the Kinetic Competency of CrHydA1 [FeFe] Hydrogenase
587 Intermediate States via Time-Resolved Infrared Spectroscopy. J. Am. Chem. Soc.
588 141, 16064–16070. <https://doi.org/10.1021/jacs.9b08348>

- 589 Sanchez, M.L.K., Wu, C.H., Adams, M.W.W., Dyer, R.B., 2019b. Optimizing electron
590 transfer from CdSe QDs to hydrogenase for photocatalytic H₂ production. *Chem.*
591 *Commun.* 55, 5579–5582. <https://doi.org/10.1039/c9cc01150a>
- 592 Seadira, T.W.P., Sadanandam, G., Ntho, T., Masuku, C.M., Scurrrell, M.S., 2018.
593 Preparation and characterization of metals supported on nanostructured TiO₂
594 hollow spheres for production of hydrogen via photocatalytic reforming of
595 glycerol. *Appl. Catal. B Environ.* 222, 133–145.
596 <https://doi.org/10.1016/j.apcatb.2017.09.072>
- 597 Shen, M., Jia, W., You, Y., Hu, Y., Li, F., Tian, S., Li, J., Jin, Y., Han, D., 2013.
598 Luminescent properties of CdTe quantum dots synthesized using 3-
599 mercaptopropionic acid reduction of tellurium dioxide directly. *Nanoscale Res.*
600 *Lett.* 8, 1–6. <https://doi.org/10.1186/1556-276x-8-253>
- 601 Song, X.W., Wen, H.M., Ma, C.B., Hu, M.Q., Chen, H., Cui, H.H., Chen, C.N., 2014.
602 Photocatalytic hydrogen evolution by two comparable [FeFe]-hydrogenase mimics
603 assembled to the surface of ZnS. *Appl. Organomet. Chem.* 28, 267–273.
604 <https://doi.org/10.1002/aoc.3119>
- 605 Stern, O., Volmer, M., 1919. Über die Abklingzeit der Fluoreszenz. *Z. Phys.* 20, 183–
606 188.
- 607 Streich, D., Astuti, Y., Orlandi, M., Schwartz, L., Lomoth, R., Hammarström, L., Ott,
608 S., 2010. High-turnover photochemical hydrogen production catalyzed by a model
609 complex of the [FeFe]-hydrogenase active site. *Chem. Eur. J.* 16, 60–63.
610 <https://doi.org/10.1002/chem.200902489>
- 611 Stripp, S.T., Happe, T., 2009. How algae produce hydrogen—news from the
612 photosynthetic hydrogenase. *Dalt. Trans.* 9960–9969.

- 613 <https://doi.org/10.1039/b916246a>
- 614 Supplis, C., Gros, F., Dahi, G., Dauchet, J., Roudet, M., Gloaguen, F., Cornet, J.F.,
615 2018. Spectral radiative analysis of bio-inspired H₂ production in a benchmark
616 photoreactor: A first investigation using spatial photonic balance. *Int. J. Hydrogen*
617 *Energy* 43, 8221–8231. <https://doi.org/10.1016/j.ijhydene.2018.03.097>
- 618 Trincado, M., Banerjee, D., Grützmacher, H., 2014. Molecular catalysts for hydrogen
619 production from alcohols. *Energy Environ. Sci.* 7, 2464-2503.
620 <https://doi.org/10.1039/c4ee00389f>
- 621 Troppmann, S., König, B., 2016. Functionalized Vesicles with Co-Embedded CdSe
622 Quantum Dots and [FeFe]-Hydrogenase Mimic for Light-Driven Hydrogen
623 Production. *ChemistrySelect* 1, 1405–1409. <https://doi.org/10.1002/slct.201600032>
- 624 Tu, Y.J., Njus, D., Schlegel, H.B., 2017. A theoretical study of ascorbic acid oxidation
625 and HOO•/O₂•⁻ Radical scavenging. *Org. Biomol. Chem.* 15, 4417–4431.
626 <https://doi.org/10.1039/c7ob00791d>
- 627 Wang, F., Liang, W.J., Jian, J.X., Li, C.B., Chen, B., Tung, C.H., Wu, L.Z., 2013.
628 Exceptional poly(acrylic acid)-based artificial [FeFe]-hydrogenases for
629 photocatalytic H₂ production in water. *Angew. Chemie Int. Ed.* 52, 8134–8138.
630 <https://doi.org/10.1002/anie.201303110>
- 631 Wang, F., Wang, W.G., Wang, H.Y., Si, G., Tung, C.H., Wu, L.Z., 2012. Artificial
632 photosynthetic systems based on [FeFe]-hydrogenase mimics: The road to high
633 efficiency for light-driven hydrogen evolution. *ACS Catal.* 2, 407–416.
634 <https://doi.org/10.1021/cs200458b>
- 635 Wang, F., Wang, W.G., Wang, X.J., Wang, H.Y., Tung, C.H., Wu, L.Z., 2011. A highly

- 636 efficient photocatalytic system for hydrogen production by a robust hydrogenase
637 mimic in an aqueous solution. *Angew. Chemie Int. Ed.* 50, 3193–3197.
638 <https://doi.org/10.1002/anie.201006352>
- 639 Wang, H.Y., Wang, W.G., Si, G., Wang, F., Tung, C.H., Wu, L.Z., 2010. Photocatalytic
640 Hydrogen Evolution from Rhenium(I) Complexes to [FeFe] Hydrogenase Mimics
641 in Aqueous SDS Micellar Systems: A Biomimetic Pathway. *Langmuir* 26, 9766–
642 9771. <https://doi.org/10.1021/la101322s>
- 643 Wang, M., Han, K., Zhang, S., Sun, L., 2015. Integration of organometallic complexes
644 with semiconductors and other nanomaterials for photocatalytic H₂ production.
645 *Coord. Chem. Rev.* <https://doi.org/10.1016/j.ccr.2014.12.005>
- 646 Wang, P., Zhang, J., He, H., Xu, X., Jin, Y., 2015. The important role of surface ligand
647 on CdSe/CdS core/shell nanocrystals in affecting the efficiency of H₂
648 photogeneration from water. *Nanoscale* 7, 5767–5775.
649 <https://doi.org/10.1039/c4nr07343f>
- 650 Wang, W., Song, X.W., Hong, Z., Li, B., Si, Y., Ji, C., Su, K., Tan, Y., Ju, Z., Huang,
651 Y., Chen, C.N., Yuan, D., 2019. Incorporation of iron hydrogenase active sites into
652 a stable photosensitizing metal-organic framework for enhanced hydrogen
653 production. *Appl. Catal. B Environ.* 258, 117979.
654 <https://doi.org/10.1016/j.apcatb.2019.117979>
- 655 Wen, M., Li, X.B., Jian, J.X., Wang, X.Z., Wu, H.L., Chen, B., Tung, C.H., Wu, L.Z.,
656 2016. Secondary coordination sphere accelerates hole transfer for enhanced
657 hydrogen photogeneration from [FeFe]-hydrogenase mimic and CdSe QDs in
658 water. *Sci. Rep.* 6, 29851. <https://doi.org/10.1038/srep29851>
- 659 Wen, M., Wu, H.L., Jian, J.X., Wang, X.Z., Li, X.B., Chen, B., Tung, C.-H., Wu, L.-Z.,

- 660 2017. Integrating CdSe Quantum Dots with a [FeFe]□Hydrogenase Mimic into a
661 Photocathode for Hydrogen Evolution at a Low Bias Voltage. *ChemPhotoChem* 1,
662 260–264. <https://doi.org/10.1002/cptc.201700041>
- 663 Wittkamp, F., Senger, M., Stripp, S.T., Apfel, U.P., 2018. [FeFe]-Hydrogenases: Recent
664 developments and future perspectives. *Chem. Commun.* 54, 5934–5942.
665 <https://doi.org/10.1039/c8cc01275j>
- 666 Wroblewska-Wolna, A.M., Harvie, A.J., Rowe, S.F., Critchley, K., Butt, J.N., Jeuken,
667 L.J.C., 2020. Quantum dot interactions with and toxicity to *Shewanella oneidensis*
668 MR-1. *Nanotechnology* 31, 134005. <https://doi.org/10.1088/1361-6528/ab5f78>
- 669 Yang, J., Miao, H., Jing, J., Zhu, Y., Choi, W., 2021. Photocatalytic activity
670 enhancement of PDI supermolecular via π - π action and energy level adjusting with
671 graphene quantum dots. *Appl. Catal. B Environ.* 281, 119547.
672 <https://doi.org/10.1016/j.apcatb.2020.119547>
- 673 Yang, Y., Zhou, C., Wang, W., Xiong, W., Zeng, G., Huang, D., Zhang, C., Song, B.,
674 Xue, W., Li, X., Wang, Z., He, D., Luo, H., Ouyang, Z., 2021. Recent advances in
675 application of transition metal phosphides for photocatalytic hydrogen production.
676 *Chem. Eng. J.* 405, 126547. <https://doi.org/10.1016/j.cej.2020.126547>
- 677 Yu, T., Zeng, Y., Chen, J., Li, Y.Y., Yang, G., Li, Y., 2013. Exceptional dendrimer-
678 based mimics of diiron hydrogenase for the photochemical production of
679 hydrogen. *Angew. Chemie Int. Ed.* 52, 5631–5635.
680 <https://doi.org/10.1002/anie.201301289>
- 681 Yu, W.W., Qu, L., Guo, W., Peng, X., 2003. Experimental determination of the
682 extinction coefficient of CdTe, CdSe, and CdS nanocrystals. *Chem. Mater.* 15,
683 2854–2860. <https://doi.org/10.1021/cm034081k>

- 684 Yue, D., Qian, X., Kan, M., Ren, M., Zhu, Y., Jiang, L., Zhao, Y., 2017. Sulfurated
685 [NiFe]-based layered double hydroxides nanoparticles as efficient co-catalysts for
686 photocatalytic hydrogen evolution using CdTe/CdS quantum dots. *Appl. Catal. B*
687 *Environ.* 209, 155–160. <https://doi.org/10.1016/j.apcatb.2017.02.075>
- 688 Zamkov, M., 2017. Solar hydrogen generation: Exceeding 100% efficiency. *Nat.*
689 *Energy* 2, 17072. <https://doi.org/10.1038/nenergy.2017.72>

690

Journal Pre-proof

Highlights of the paper “*Influence of QD photosensitizers in the photocatalytic production of hydrogen with biomimetic [FeFe]-hydrogenase. Comparative performance of CdSe and CdTe*”:

- Photocatalytic hydrogen production system with [Fe-Fe]H₂-ase mimic, and CdSe or CdTe QDs as photosensitizers.
- Comparison of CdSe and CdTe QDs performance as photosensitizers
- CdSe showed the best performance for hydrogen production.
- Electron transfer rate from ascorbic acid to QDs and from QDs to catalysts has been investigated.
- Electron transfer rate from ascorbic acid to QDs was found as rate limiting step.

Declaration of interests

- The authors declare that they have no known competing financial interests or personal relationships that could have appeared to influence the work reported in this paper.
- The authors declare the following financial interests/personal relationships which may be considered as potential competing interests:

Journal Pre-proof